JOURNAL OF COMPUTATIONAL PHYSICS 117, 289–299 (1995)

Implementation of a Nonlinear Filter with a Lagrangian Formulation for the Treatment of Very High Pressure Reflected Shocks

C. K. B. LEE

Logicon RDA, Los Angeles, California

AND

J. M. MCDONOUGH

University of Kentucky, Lexington, Kentucky

Received December 6, 1993

The Engquist filter is implemented within the one-dimensional Lagrangian gas dynamics code HAROLD. The conservation version and the total variation diminishing version of the filter are combined as proposed in the original paper, with filtering performed in characteristics space. The present results show that the filter performs well in the Lagrangian system for very strong shocks. A new treatment of the wall boundary reflection for strong shocks that takes advantage of the filter is presented. Reflected shocks calculated using this technique show essentially no overshoots typical of classical finite-difference codes. These results show promise in applying the filter and the characteristics scheme to more complicated gas dynamics problems not only because of the high quality of the solutions, but also because the additional run time incurred due to the filter is minimal. Furthermore, it follows that older codes formulated using second-order finite difference methods utilizing artificial viscosity can be converted into accurate, modern tools with a high potential for parallelizability.

1. INTRODUCTION

The period from the mid 1970s through the late 1980s may be considered as one of the most important periods in the development of advanced numerical methods for solving the nonlinear system of conservation laws in gas dynamics. This is the period during which most of the ideas, set out to change the basic approach to shock capturing consisting of classical finite-difference methods combined with the use of artificial viscosity [1], came to fruition. The deficiencies associated with the classical finite-difference schemes result in either sharp shocks with spurious oscillations as seen, for example, in the Lax–Wendroff schemes, or smeared shocks for which the artificial viscosity (added, or naturally presented) causes permanent loss of information, as in the basic first-order Godunov methods. Most of the "higher-order" numerical methods put forth during this period are capable of producing sharp shocks with very little Gibbs oscillation for one-dimensional shock tube problems, and they have been extended (with some difficulty) to higher-dimensional problems of greater complexity. They include: flux-corrected transport (FCT) [2], total variation diminishing (TVD) [3], and the piecewise-parabolic method (PPM) [4]. Although the genesis of these schemes is quite different, the main idea behind them is the same: to introduce judicious amounts of dissipation at chosen spatial locations at or near the shock front to reduce the magnitude of, or eliminate, the spurious oscillations without smearing the shock. In general, these schemes do not allow oscillations at the shock, and for this reason, they reduce to first order (or even zeroth order) at the shock, even though the underlying basic numerical scheme may be as high as third order. By allowing a small amount of oscillation at the shock front, the subsequently proposed essentially nonoscillatory (ENO) scheme [5] can achieve $(q-1)^{\text{th}}$ order of accuracy at the shock for a q^{th}-order scheme.

The number of schemes of the above-mentioned sort that have been introduced in recent years has been truly overwhelming, and we shall not attempt a thorough review in the present paper. But because of this great variety of available shock-capturing methods it is important to recognize the factors that should be considered in selecting one for application to any specific class of problems. First, it is well known that most TVD schemes, even if cleverly implemented, will result in at least a factor of two increase in CPU time, and as much as an order of magnitude increase if not well implemented, in comparison with finite-difference methods employing simple artificial viscosity approaches. ENO schemes generally require more arithmetic than do TVD schemes. Second, it is difficult (although certainly not impossible) to retrofit an existing code with one of the new higher-order methods, so it is often better to construct a new code. This, however, imposes additional code validation tasks that are, in general, very time consuming.

0021-9991/95 $6.00

Thus, development of a completely new code represents a significant investment of resources. Within this context, the nonlinear Engquist filter [6], and the subsequently proposed ENO filters [7], offer an interesting alternative. Engquist *et al.* observed that judicious amounts of dissipation introduced at a few chosen spatial locations at or near a shock can be achieved by a simple filter, implemented in conjunction with a finite-difference code as a postprocessing step. The increase in run time as a result of the filter should be small because, hopefully, only a small number of spatial nodes need to be corrected. Compared to the higher-order codes [2–4], this technique has to be less costly. In principle, the filter can be applied to results from any existing higher-order scheme. A simple inexpensive screening routine can then be used at each time step to determine which nodes need to be corrected. As already hinted, the screening (seeking nonphysical local extrema) and the corrections can be easily implemented in existing codes. We comment that each of these points has been demonstrated in [6] for relatively simple one- and two-dimensional problems in an Eulerian reference frame.

The objective of this paper is to demonstrate that the Engquist filter can be implemented in a straightforward way in the old HAROLD [8] code (vintage 1967). HAROLD was the first code used to compute airblasts from nuclear explosions. We wish to emphasize that there are three key aspects of this study that are new and, to the authors' knowledge, have not previously been described. These are: (1) application of the Engquist filter in the context of a Lagrangian formulation of the equations of motion; (2) treatment of problems involving very strong (by aerodynamic standards) shock overpressure $\geq$0.1 GPa shocks; and (3) modification of the method to permit calculation of these strong shocks undergoing reflection at a solid boundary.

For the purpose of this paper we will limit our discussion to the gas dynamics problem, although HAROLD was originally formulated for modeling the radiation hydrodynamics of shocked air created by a nuclear explosion. The problem including radiation is the subject of another endeavor. In the following sections, we will first present the basic equations solved in HAROLD without the radiation term, followed by the characteristics analysis employed for the system version of the Engquist filter. Then we will discuss the difference equations and the artificial viscosity used in HAROLD. We next present the algorithm corresponding to our version of the Engquist filter and a treatment of shock reflection at a solid wall boundary, taking advantage of the properties of the filter. Finally, we present and discuss the results of this study. While the methods utilized in HAROLD are well known, we feel that it is advantageous to provide a complete, self-contained treatment in this paper; but the basic material will be presented here in abbreviated form.

2. ANALYSIS

As mentioned in the Introduction, HAROLD is a radiation hydrodynamics code that solves the one-dimensional Lagrangian form of the conservation equations in spherical and planar geometry. For the purpose of this paper we are interested in the planar version of HAROLD without the radiation. Our nomenclature is the same as that of the original report for HAROLD [8]. To develop the local characteristics required to implement the Engquist filter for systems we start from the planar Lagrangian equations

$$V = \frac{\partial R}{\partial m}, \tag{1}$$

$$\frac{\partial u}{\partial t} = \frac{\partial P}{\partial m}, \tag{2}$$

$$\frac{\partial I}{\partial t} = -P\frac{\partial V}{\partial t}. \tag{3}$$

Here V is the specific volume, R is the distance, u is the velocity, P is the pressure, I is the internal energy, m is the mass, and t is the time. The equation of state is that of a gamma-law gas with $\gamma = 1.4$.

The initial and boundary conditions are

$$\begin{aligned} V(R, 0) &= V_0, \\ u(R, 0) &= 0, \\ P(R, 0) &= P_0, \end{aligned} \tag{4}$$

with $V_0 = 909.1$ cm^3/g and $P_0 = 9.275 \times 10^{-5}$ GPa for all R, and for $t > 0$ a pressure P_{in} is applied at the left boundary (R_l), i.e.,

$$P(R_l, t) = P_{\text{in}}. \tag{5}$$

For the case of shock reflection, a wall boundary condition is imposed at the right boundary ($R = 1.45$ m for the case presented in Section 4.0):

$$u(R_r, t) = 0. \tag{6}$$

For the system of Eqs. (1), (2), and (3) we define the independent variable vector $\mathbf{U}$ and the flux vector $\mathbf{F}$ as

$$\mathbf{U} = \begin{bmatrix} 1/\rho \\ u \\ E \end{bmatrix}, \quad \mathbf{F} = \begin{bmatrix} -u \\ \rho(\gamma - 1)\left(E - \dfrac{u^2}{2}\right) \\ \rho u(\gamma - 1)\left(E - \dfrac{u^2}{2}\right) \end{bmatrix}, \tag{7}$$

where $\rho = 1/V$ and E is the total energy. The associated acoustic matrix is

$$\mathbf{A} = \frac{\partial \mathbf{F}}{\partial \mathbf{U}} = \begin{bmatrix} 0 & -1 & 0 \\ -\rho^2(\gamma-1)\left(E-\frac{u^2}{2}\right) & -\rho u(\gamma-1) & \rho(\gamma-1) \\ -\rho^2(\gamma-1)u\left(E-\frac{u^2}{2}\right) & \rho(\gamma-1)\left(E-\frac{3u^2}{2}\right) & \rho u(\gamma-1) \end{bmatrix}. \tag{8}$$

The eigenvalues λ_i, $i = 1, 2, 3$, for $\mathbf{A}$ are 0, and $\pm\rho c$, with c being the sound speed, in agreement with Courant and Friedrichs [9]. The corresponding eigenvectors are given by

$$[\mathbf{A} - \lambda_i I]\mathbf{e}_i = 0. \tag{9}$$

In our computations $\mathbf{A}$ is an extended form of the Roe matrix [10] to Lagrangian systems. We observe that the third component of the flux vector $\mathbf{F}$, F_3, is the negative of the product F_1F_2. Hence, the jump condition for F_3 can be represented by ΔF_1 and ΔF_2 exactly, while the physical quantities needed to evaluate ΔF_1 and ΔF_2 are Roe averaged.

3. NUMERICAL ANALYSIS

In this section we provide details of the numerical methods employed in this study. We begin by presenting the finite-difference discretizations of Eqs. (1) through (3), as they have been employed in HAROLD. We then discuss the basic extensions we have made to the Engquist filter and provide a detailed analysis of our treatment of shock reflections in the context of our basic filter, in particular noting subtle aspects of the implementation that have not been addressed by previous authors. We then present the pseudo-language algorithm for implementing this procedure.

3.1. Difference Equations in HAROLD

For completeness we present the second-order accurate finite difference equations used in HAROLD. They are

$$V_{j-1/2}^{n+1} = \frac{R_j^{n+1} - R_{j-1}^{n+1}}{\Delta m_{j-1/2}} = \frac{1}{\rho_{j-1/2}^{n+1}} \tag{10}$$

$$u_j^{n+1/2} = u_j^{n-1/2} - \frac{\Delta t^n}{\Delta m_j}(P_{j+1/2}^n - P_{j-1/2}^n + Q_{j+1/2}^{n-1/2} - Q_{j-1/2}^{n-1/2}) \tag{11}$$

$$E_{j-1/2}^{n+1} = E_{j-1/2}^n + (\tfrac{1}{2}P_{j-1/2}^{n+1} + \tfrac{1}{2}P_{j-1/2}^n + Q_{j-1/2}^{n+1/2})(V_{j-1/2}^n - V_{j-1/2}^{n+1}), \quad j = 2, 3, \ldots, j_{\max}, \tag{12}$$

where

$$\Delta m_j = \tfrac{1}{2}\Delta m_{j+1/2} + \tfrac{1}{2}\Delta m_{j-1/2}, \tag{13}$$

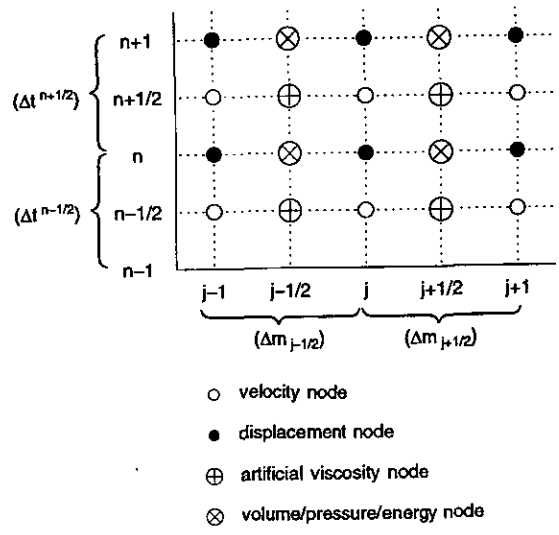

FIG. 1. Staggered centered difference grid for Lagrangian HAROLD code.

$$\Delta t^n = \tfrac{1}{2}\Delta t^{n+1/2} + \tfrac{1}{2}\Delta t^{n-1/2}, \tag{14}$$

$$R_j^{n+1} = R_j^N + u_j^{n+1/2}\,\Delta t^{n+1/2}, \tag{15}$$

and the artificial viscosity (the so-called quadratic Q) is

$$Q_{j-1/2}^{n+1/2} = \frac{C_1\,\Delta m_{j-1/2}^2 (V_{j-1/2}^{n+1} - V_{j-1/2}^n)^2}{(V_{j-1/2}^{n+1} + V_{j-1/2}^n)(\Delta t^{n+1/2})^2} \tag{16}$$

for $V^{n+1} < V^n$, zero otherwise. Note that there is a linear Q option in HAROLD, but we have not used it in the present study. Figure 1 shows the staggered grid used in HAROLD.

3.2. The Engquist Filter

Our version of the nonlinear filter is an extension of Engquist's algorithm 4.1 [6] which has the conservative property only. We extended Engquist's algorithm 4.1 to include a TVD property in the characteristic variables, but as mentioned in [6], this method of implementation does not guarantee the TVD property for the physical variables. On the other hand, the cost of using a full TVD filter is substantially higher. Therefore, we have chosen to implement a "semi-TVD" version of the filter and to perform a set of numerical experiments to study its performance. Generally, the filter has performed well. Occasionally, however, we do encounter cases where the TVD property in the physical variables is violated; namely, pressure overshoots are obtained after the physical variables are processed by the filter. These increases are typically so small that they usually vanish during the next few timesteps, but in some cases associated with shock reflections they persist at very low amplitude. In addition to this we have incorporated vector versions of the Engquist *et al.* [6] scalar algorithms for removing plateaus and "zigzags," and we have implemented a treatment

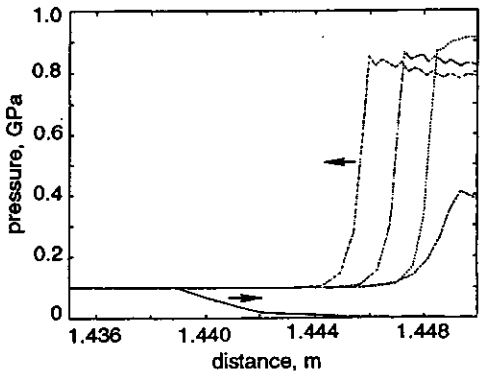

FIG. 2. Typical overshoot in reflected pressure in HAROLD; the theoretical reflected pressure is 0.795480401556 GPa.

to handle shock reflections at solid boundaries. In the following subsections we will present a fairly detailed treatment of the last of these, namely the shock reflection problem, and briefly discuss the other items in the course of providing some explanatory notes associated with the pseudo-language algorithm for the complete procedure.

3.2.1. *Treatment of Shock Reflection at a Wall*

Both the conservation form and the TVD form of the Engquist filter are designed to smooth out oscillations arising from the Gibbs phenomenon at a jump discontinuity. We might expect that the oscillations with wavelengths of the order of the grid spacing would be filtered, but those with long wavelengths, on the order of several grid spacings would be unaffected by the filter. Indeed, Shyy et al. [11] recently reported a study of the development of numerical oscillations and their interaction with the conservative filter. They concluded that spurious oscillations with wavelengths larger than twice the grid cannot be removed by the filter.

We have taken advantage of this property of the filter in our treatment of the wall reflection. It is well known that finite difference techniques applied to a shock reflection generally produce a pressure overshoot that remains in the solution even when the reflected shock is tens of grid points away from the wall. The overshoot in HAROLD is typically about 15% higher than the value of the analytical solution, as displayed in Fig. 2. Our strategy is to reduce the artificial viscosity at the wall to the extent that larger-amplitude (~20%), higher-frequency oscillations are produced, thus leading to short-wavelength spatial oscillations. These oscillations will propagate away from the wall following the reflected shock, and we then use the filter to eliminate these short-wavelength oscillations.

In the finite difference formulation, the pressure overshoot is caused by two numerical artifacts. The first one is the gradual pressure increase in front of the shock (cf. parts a of Figs. 3 and 4 below). When this gradual rise reaches the wall, it reflects to a higher pressure, changing the condition at the wall before the arrival of the peak value associated with the actual shock. The second effect has to do with the artificial viscosity at the wall when the shock approaches. It is well known [1] that in the region just ahead of the first peak where the rise in pressure is very sharp, the artificial viscosity is much larger than the pressure. Before the first peak of the shock reaches the wall, this region of sharp rise delivers a large amount of artificial viscosity to the Lagrangian zone adjacent to the wall. We can see the specific cause of this overshoot by rewriting Eq. (12) at the wall cell

$$E_{\text{wall}}^{n+1} = E_{\text{wall}}^{n} + \tfrac{1}{2}(P_{\text{wall}}^{n+1} + P_{\text{wall}}^{n} + 2Q_{\text{wall}}^{n+1/2})(V_{\text{wall}}^{n} - V_{\text{wall}}^{n+1}), \quad (17)$$

and the equation of state

$$E_{\text{wall}} = \frac{P_{\text{wall}} V_{\text{wall}}}{\gamma - 1}, \quad (18)$$

where subscript "wall" denotes the zone adjacent to the wall. When the region of sharp rise arrives at the wall $Q_{\text{wall}}^{n+1/2}$ is much larger than $(P_{\text{wall}}^{n+1} + P_{\text{wall}}^{n})/2$, causing E_{wall}^{n+1} to experience a nonphysical overshoot, and from Eq. (18) so also will P_{wall}. Several time steps later, $P_{\text{wall}} - P_{j_{\max}-1/2}$ becomes so large that it reverses the velocity $u_{j_{\max}-1}$ (the node adjacent to the wall) via Eq. (11) causing a drop in P_{wall} as well as an increase in V_{wall}. This drop in P_{wall} causes a mild velocity reversal and the process repeats. As $u_{j_{\max}-1}$ approaches zero, P_{wall} also stabilizes while the reflected shock propagates away from the wall. Unfortunately, this overshoot in the pressure occurs over approximately five grid points for most of our test problems, meaning that the filter cannot effectively eliminate the overshoot.

There are a number of ways that one could change the wavelength of the overshoot. The most effective way we found is by allowing only the peak of the incident shock to reach the wall. The sharp rise ahead of the shock is eliminated by setting $Q_{\text{wall}}^{n-1/2}$ equal to $-P_{\text{wall}}^{n}$ in Eq. (11) for the node next to the wall until the peak of the incident shock reaches the wall, i.e., $P_{\text{wall}} \geq P_{\text{incident}}$. At this point, $Q_{\text{wall}}^{n-1/2}$ is allowed to return to zero according to

$$Q_{\text{wall}}^{n-1/2} = -P_{\text{wall}}^{n} e^{-(t-t_{\text{ref}})/\Delta t_{\text{ref}}}, \quad (19)$$

where the reflection time t_{ref} is defined as the time at which $P_{\text{wall}} = P_{\text{incident}}$, and Δt_{ref} is the time step at t_{ref}. We left the energy equation at the wall (Eq. (17)) unchanged to ensure that the pressure oscillations at the wall are sufficiently small to be removed effectively by the filter. Our numerical experiments show that somewhat more time steps are needed to complete the reflection than might be expected simply on the basis of satisfying a Courant condition. This is caused by a reduction in the time step itself throughout the reflection. The long wavelength overshoot caused by the rise to the peak pressure at the wall and the associated artificial viscosities is converted to a

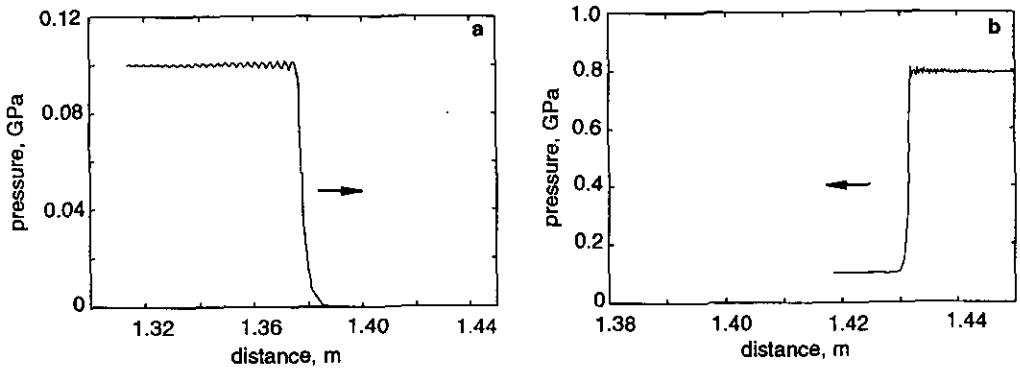

FIG. 3. Unfiltered second-order finite difference solution from one-dimensional Lagrangian code HAROLD with proposed change in treatment of wall reflection: (a) incident shock; and (b) reflected shock.

set of short wavelength oscillations that the filter eliminates in the next approximately 20 time steps (the reflected shock by this time is less than 10 grid points away from the wall).

We again emphasize that this seemingly ad hoc procedure is designed to exploit the basic properties of the filter. As a consequence, it is expected to be useful mainly in the context of filter implementations such as we are treating here, and possibly for higher-order filters discussed in [5]. Nevertheless, as indicated in Fig. 3, some improvement can be seen even in the basic HAROLD results without the filter.

3.2.2. *Filtering Procedure*

For the incident shock, the filter starts from node 2 and stops five nodes ahead of the node, where the largest artificial viscosity is calculated. We call this the *filter region.* The front of this region is generally eight nodes ahead of the peak of the shock. If the length of the filter region is larger than $j_{\max}$, the filter will only operate on nodes 2 to $(j_{\max} - 1)$; i.e., we do not permit the filter to adjust boundary values. We also note that the finite difference solution produced by HAROLD gives specific volumes and internal energies that are incorrect at the boundary (even though the solution quickly becomes correct a couple of nodes from either boundary, see Fig. 8), thus introducing errors into the solution through the characteristics that are routinely employed in the filter. The fact that the specific volumes and internal energies are incorrect at boundaries is well known, and these discrepancies can be traced back to the errors introduced by the artificial dissipation when the shock is at the boundary. We handle this in the context of the filter implementation in the following way.

As the peak of the shock approaches the wall boundary, the nodes near that boundary will begin to move toward the wall in a Lagrangian formulation. When the node adjacent to the wall attains a velocity larger than 0.01 km/s we turn off the filter until the velocity at this node drops back to below this value after the reflection. During this time, the physical quantities exhibit rapid temporal oscillations that are not easily removed by the filter because the filter is designed to handle spatial oscillations at a fixed time rather than time-dependent oscillations at a point in space. Thus, we simply avoid applying the filter in situations where it cannot be effective. After the reflection, we reverse the arrays of physical quantities such that

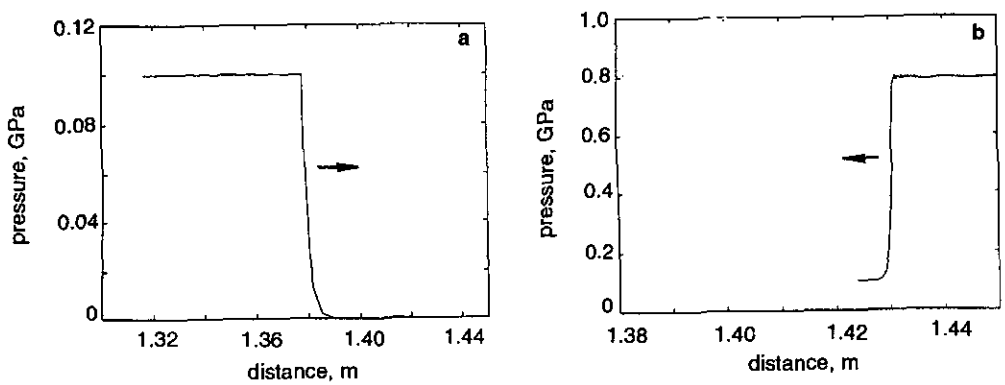

FIG. 4. Filter applied to incident shock: (a) incident shock—no Gibbs oscillations but long wavelength oscillations of less than 0.5% relative amplitude; and (b) reflected shock—oscillations less than 1.5% relative amplitude.

the positive R direction is pointing away from the wall. Again the filter is applied with the filter region defined in the same way as for the incident shock. Our experience with this filter is that it performs well when applied from behind the shock, sweeping up to five nodes ahead of the maximum in the calculated artificial viscosity. The direction of the filter sweep must be the same as that of the particle velocity vector.

We close this section with the pseudo-language algorithm corresponding to our implementation of the Engquist *et al.* filter. Most of the salient features of this algorithm have already been described, but we do wish to note the implementation of code to permit the treatment of plateaus and zigzags in the case of systems of equations which have not been reported previously. This is handled in a manner that is analogous to what was done by Engquist *et al.* [6] for the scalar case. In particular, it enters into the correction factor δ, which in the case of systems is obtained by limiting the characteristic variables.

We also comment that the physical variable that enters the Filter subroutine in the z-array and which, therefore, determines which points will be filtered, differs between the incident and reflected shock. In the former, the velocity is used to trigger the filter, while in the reflected shock case, we found that using the specific volume improved the results. Finally, we note that, although the algorithm has been written specifically for the case of only three independent variables, the extension to larger numbers of variables is straightforward.

ALGORITHM. (HAROLD with modified Engquist *et al.* filter). Assume n time steps have been completed. To calculate results at time level $n + 1$, perform the following computations.

1. Use basic HAROLD code to calculate advanced time level results.

Do $j = 2, j_{\max} - 1$
If $j + 2 = j_{\max} + 1$ then
[Adjust artificial viscosity to prevent overshoots during shock reflection]
$Q_{\text{wall}} = Q_{j_{\max}+1}$
If $P_{j_{\max}+1} < P_1$ [Incident shock has not reached right boundary] then
$Q_{j_{\max}+1} = -P_{j_{\max}+1}$
$Q_{\text{wall}} = Q_{j_{\max}+1}$
$t_{\text{ref}} = t$
$\Delta t_{\text{ref}} = \Delta t$
else
$Q_{j_{\max}+1} = -P_{j_{\max}+1} e^{-(t-t_{\text{ref}})/\Delta t_{\text{ref}}}$
$Q_{\text{wall}} = Q_{j_{\max}+1}$
endif
endif
Calculate u_j, r_j, $V_{j-1/2}$ from Eqs. (10), (11), (13) through (15), and update $Q_{j-1/2}$ using Eq. (16).
enddo

2. Calculate internal energy from Eq. (12) and pressure from equation of state.

3. Apply Engquist *et al.* filter
$n_{\text{ref}} = 0$
If $P_{j_{\max}+1} > P_1$ [Incident shock has reached right boundary] then
$n_{\text{ref}} = 1$
Reverse indexing of solution arrays; switch signs on velocity between shock location and right boundary
endif
[Set length of filter region]
$j_{\text{peak}} = 2$
$j_{\text{plus}} = 5$ [Entered as input]
Do $j = 2, j_{\max} + 1$
If $2Q_j - P_j > 0$ then
$j_{\text{peak}} = j$
goto A.
endif
enddo
A. $j_{\text{filter}} = j_{\text{peak}} + j_{\text{plus}}$
If $n_{\text{ref}} = 1$ [Shift reversed strings by 1 to prevent filtering at boundary] then
$j_{\text{filter}} = j_{\max} + j_{\text{plus}} - j_{\text{peak}} + 2$
endif
If $u_{j_{\max}} < 0.01$ then
If $j_{\text{filter}} > 10$ and $n_{\text{ref}} = 0$ [Filter incident shock]
Call Filter $(u, u_n, j_{\text{filter}})$
If $j_{\text{filter}} > j_{\max} + 1$ **and** $n_{\text{ref}} = 1$ [Filter reflected shock] then
Call Filter $(V, V_n, j_{\text{filter}})$
Back-shift and reverse data strings; switch signs on velocity between shock and right boundary
endif
endif

Subroutine Filter (z, z_n, n)
[Modified, "semi-TVD" Engquist *et al.* filter]
$j_{\text{skip}} = 2$
Call newndx $(z, j_{\text{skip}}, l, j, n)$
$j_{\text{strt}} = j$
Do $j = j_{\text{strt}}, n - 1$
$\delta = 0$
If $j > j_{\text{strt}}$ then
$l_{\text{sve}} = l$
$j_{\text{sve}} = j$
Do $k = 1, 3$
$\Delta^{(\alpha)}_{+,\text{sve}}(k) = \Delta^{(\alpha)}_{+}(k)$
$\Delta^{(\alpha)}_{-,\text{sve}}(k) = \Delta^{(\alpha)}_{-}(k)$
enddo $[k]$
$\omega_{1,\text{sve}} = \omega_1$
$\omega_{2,\text{sve}} = \omega_2$
Call newndx (z, j, l, j, n)
endif
Call vmnmx $(z_n, z_{n,\min}, z_{n,\max}, l - 1, j + 1)$
$d_1 = z_j - z_{n,\max}$
$d_2 = z_{n,\min} - z_j$

$\Delta_+ = z_{j+1} - z_j$
$\Delta_- = z_l - z_{l-1}$
If $\Delta_+\Delta_- < 0$ and ($d_1 > 0$ or $d_2 > 0$) then
Call alpha (α_+, α_-, $l - 1$, $j + 1$) [Compute characteristic variables]
Do $k = 1, 3$ [Use α's scalarly]
$\Delta_+ = \alpha^{(j)}_{+,k}$
$\Delta_- = \alpha^{(l)}_{-,k}$
$\Delta^{(\alpha)}_+(k) = \Delta_+$
$\Delta^{(\alpha)}_-(k) = \Delta_-$
[Remove plateaus]
If $\Delta_+\Delta_- < 0$ then
$d_1 = 0$
$d_2 = 0$
$s = \text{sgn}(\Delta_+)$
If $|\Delta_+| > |\Delta_-|$ then
$\delta_+ = |\Delta_+|$
$\delta_- = |\Delta_-|$
$j_{\text{correct}} = j + 1$
$l_{\text{correct}} = j + 1$
else
$\delta_+ = |\Delta_-|$
$\delta_- = |\Delta_+|$
Call newndx (z, $l - 1$, l_{correct}, j_{correct}, n)
endif
$\omega_1 = j - l + 1$
$\omega_2 = j_{\text{correct}} - l_{\text{correct}} + 1$

$$\delta = \min\left[\delta_-, \frac{\omega_2\delta_+}{\omega_1 + \omega_2}\right]$$

$\delta = \max[\delta, \max(d_1, d_2)]$
[Add filtered transformed characteristic variables to dependent variable vector to guarantee conservation]
Do $i = l, j$
$V_i = V_i + s\,\delta e^{(i)}_{1,k}$
$u_i = u_i + s\,\delta e^{(i)}_{2,k}$
$E_i = E_i + s\,\delta e^{(i)}_{3,k}$
enddo [i]
Do $i = l_{\text{correct}}, j_{\text{correct}}$ [Apply corrections to plateau region]
$V_i = V_i - s\,\delta e^{(j)}_{1,k}$
$u_i = u_i - s\,\delta e^{(j)}_{2,k}$
$E_i = E_i - s\,\delta e^{(j)}_{3,k}$
enddo [i]
endif
enddo [k]
elseif $j > j_{\text{strt}}$ and $\Delta_+\Delta_- < 0$ and $\Delta^{(\alpha)}_{+,\text{sve}}\Delta^{(\alpha)}_{-,\text{sve}} < 0$ then
[Remove zigzags]
Call alpha (α_+, α_-, e, $l - 1$, $j + 1$)
Do $k = 1, 3$
$\Delta_+ = \alpha^{(j)}_{+,k}$
$\Delta_- = \alpha^{(l)}_{-,k}$
$\Delta^{(\alpha)}_+(k) = \Delta_+$
$\Delta^{(\alpha)}_-(k) = \Delta_-$
$s = \text{sgn}(\Delta_+)$
$\omega_1 = j - l + 1$

$$\delta = \frac{\omega_{2,\text{sve}}\left|\Delta^{(\alpha)}_{+,\text{sve}}(k)\right|}{\omega_{1,\text{sve}} + \omega_{2,\text{sve}}}$$

$\delta = \min[|\Delta^{(\alpha)}_{-,\text{sve}}(k)|, 0.5|\Delta^{(\alpha)}_{+,\text{sve}}(k)|, \delta]$
Do $i = l, j$
$V_i = V_i + s\,\delta e^{(i)}_{1,k}$
$u_i = u_i + s\,\delta e^{(i)}_{2,k}$
$E_i = E_i + s\,\delta e^{(i)}_{3,k}$
enddo [i]
Do $i = l_{\text{sve}}, j_{\text{sve}}$ [Apply corrections to remove zigzags]

$$V_i = V_i - \frac{\omega_{1,\text{sve}}}{\omega_{2,\text{sve}}} s\,\delta e^{(j)}_{1,k}$$

$$u_i = u_i - \frac{\omega_{1,\text{sve}}}{\omega_{2,\text{sve}}} s\,\delta e^{(j)}_{2,k}$$

$$E_i = E_i - \frac{\omega_{1,\text{sve}}}{\omega_{2,\text{sve}}} s\,\delta e^{(j)}_{3,k}$$

enddo [i]
enddo [k]
Call jcntr (j, l)
endif
If $\delta = 0$ then
$\omega_1 = 1$
$\omega_2 = 1$
endif
enddo [j]
Return

Subroutine newndx (z, i, i_{mn}, i_{mx}, n)
[ε set to machine-ε]
$i_{mn} = i$
$i_{mx} = i$
Do $j = i + 1, n - 1$
If $|z_i - z_j| < \varepsilon$, $i_{mx} = j$
If $|z_i - z_{j+1}| > \varepsilon$, **goto** A
enddo [j]
A. **Do** $j = i - 1, 2, -1$
If $|z_i - z_j| < \varepsilon$, $i_{mn} = j$
If $|z_i - z_{j-1}| > \varepsilon$, **goto** B
enddo [j]
B. **Return**

Subroutine vmnmx (z, $z_{\min}$, $z_{\max}$, i_{mn}, i_{mx})
$z_{\min} = z_{i_{mn}}$
$z_{\max} = z_{i_{mx}}$
Do $i = i_{mn} + 1, i_{mx}$
If $z_i < z_{\min}$, $z_{\min} = z_i$
If $z_i > z_{\max}$, $z_{\max} = z_i$
enddo [i]
Return

Function jcntr (j, l)
$j = l - 1$
Return

Subroutine alpha (α_+, α_-, e, $l-1$, $j+1$)
[This subroutine calculates characteristic coordinates and basis vectors corresponding to $\Delta_\pm V_j$, $\Delta_\pm u_j$, $\Delta_\pm E_j$ via Eqs. (7) through (9).]

4. RESULTS AND DISCUSSION

All results to be reported herein were obtained using an IBM RS6000 workstation running double precision Fortran 77. Unless specifically stated to the contrary, the spatial (actually mass in the Lagrangian system) grid contained 90 points.

We started the present study utilizing a strong (0.1 GPa) shock that is of interest in the analysis of effects of high-energy explosions. For this case, a number of runs were made to study the interaction between the artificial viscosity and the filter. Our results indicate that for strong shocks (>0.01 GPa) a small amount of Q is needed to reduce the magnitudes of the Gibbs oscillations to a level that can be effectively filtered. If the amplitude of the oscillations exceeds a certain threshold, no amount of filtering can eliminate them. (We note that this is in accord with the remarks by Engquist *et al.* [6].) Our experience is that the large-amplitude, long-wavelength oscillations (wavelength longer than two grid spacings) will reduce in amplitude, but at the same time widen in wavelength to span several grid points, forming plateaus. As pointed out by Shyy *et al.* [11], these larger wavelength oscillations are transparent to the filter. In this strong shock regime, the finite difference solution is unable to stably evolve these low frequency plateaus for any length of time. The computed solution usually exhibits floating point overflow shortly after the appearance of the plateaus. In such cases, a small but judicious amount of artificial viscosity to limit the amplitudes of the initial oscillations makes the filter much more effective. On the other hand, an excessive amount of artificial viscosity not only reduces the sharpness of the computed shock but also causes problems when the filter attempts to sharpen it. In this case, the shock front first shows a step in front of the peak. Then the entire front turns into a staircase before the solution overflows. There is an optimal amount of artificial viscosity that we were able to identify in each case so as to obtain the sharpest shock front but minimal oscillation amplitudes. It should be noted that this changes from problem to problem, and we feel it is an open question as to whether the optimal level of artificial viscosity can be theoretically specified, a priori, or even determined adaptively.

Based on the above experience with the filter, our strategy in computing strong shocks is as follows. First, identify the smallest Q needed to produce a finite-difference solution with the shock resolved in two to three nodes. The largest amplitude of the pressure oscillation should not exceed 20% of the peak pressure. Then apply the filter and let the filter smooth out the oscillations and sharpen the shock.

Figure 3a shows the incident shock computed with HAROLD without filtering for the case posed in Section 2. The left boundary is at 1 m, and the right boundary is at 1.45 m. In this case, the oscillations are approximately 3% of the peak value, but the shock front is not very sharp. From Fig. 3b, it is clear that with the wall boundary modified according to Section 3.3 there is no overshoot other than the usual Gibbs oscillations in the reflected shock. Figures 4a and b show the corresponding filtered incident and reflected shock. The incident shocks are sharpened and the oscillations removed. The amplitude of the oscillations in the reflected shock shown in Fig. 4b is also reduced, but not entirely eliminated. This suggests that the larger oscillation amplitude observed in the unfiltered case (Fig. 3) is, in part, due to the oscillations in the incident shock. Again, there is very little overshoot, but more importantly, there are no long wavelength oscillations in the reflected shock.

Figure 5 shows the case with the filter applied to both the incident and the reflected shock. The pressure oscillations in the reflected shock are as small (percentage-wise) as those in the incident shock. It is interesting to note here that the CPU time required to compute this solution was 145 s, compared with 102 s for a run to the same point in physical time without the filter, representing an increase due to the filter of less than 50%.

Next, we conducted a convergence study and obtained a grid

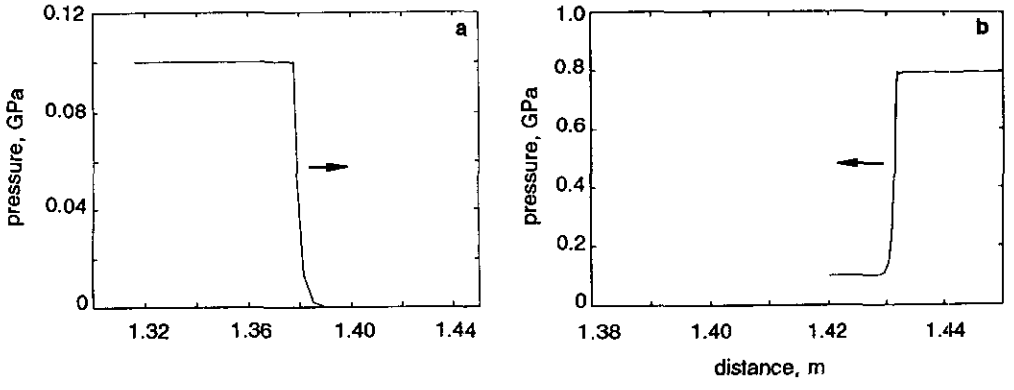

FIG. 5. Filter applied to both (a) incident and (b) reflected shock. Fully developed reflected shock contains long wavelength oscillations of less than 0.5% relative amplitude.

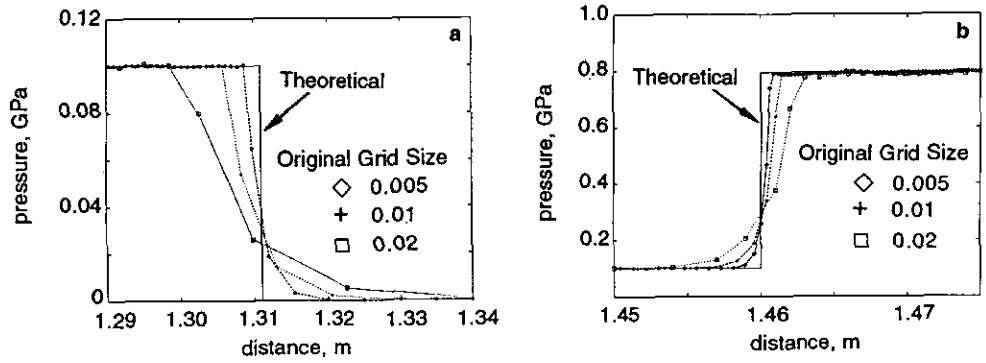

FIG. 6. Grid function convergence of filtered solution.

function convergence rate corresponding to first-order accuracy in the L^1-norm with respect to refinement of the mass density grid for the incident and reflected shocks. At the shock front the sharpest rise in pressure is usually resolved in two nodes. In Fig. 6 we present results of these grid function convergence tests at two different times in the calculations; part a of the figure corresponds to the incident shock, while part b provides similar results for the reflected shock. It is of interest to note that both figures show a first-order convergence rate and high resolution on the finer grid spacings, indicating that our boundary treatment of the shock reflection is very effective. We remark that for weak solutions, of the sort being computed here and for TVD-like schemes, the best we should expect is for the number of grid points required to capture the shock to remain constant, independent of grid spacing, as is the case for both the incident and reflected shock. In particular, the second-order accuracy often quoted for TVD schemes is attained only outside a neighborhood of any shocks that are present (cf. [5]). In the current problem, the solution is constant away from the shock, so our observed first-order accuracy in the L^1-norm simply reflects the fact that the filter has the same accuracy in the neighborhood of the shock as would any other TVD method. The second-order accuracy of the filter has already been demonstrated for problems with nonconstant, smooth solutions away from shocks by Engquist *et al.* [6]. This in turn implies that as the grid is refined, shock resolution will improve. Figure 6 displays results computed with grid spacings of 0.02, 0.01, and 0.005 for the spatial domain described earlier. As can be seen, five grid points are needed to capture the shock on all three grids.

For completeness, we show in Fig. 7 the artificial viscosity for the zone adjacent to the wall. Figure 7a shows the amount subtracted from the pressure at grid cell $j_{\max} - 1$. Before the wall pressure reaches the magnitude of Q for the incident shock, Q for the momentum equation is set to the negative of the pressure at the $j_{\max} - 1$ cell such that the wall, in terms of momentum, does not experience any preconditioning by the pressure rise ahead of the incident peak (i.e., it is not affected by the finite thickness of the numerical shock). When the incident peak pressure reaches the wall, the impact generates only high frequency oscillations at the wall, and these are converted to short wavelength oscillations in the reflected shock. These oscillations are then removed by the filter. The artificial viscosity for the energy equation is shown in Fig. 7b. This is the same as in Eq. (16).

Figures 8 and 9 are the corresponding specific volumes and velocities for the filtered solution. As noted before, the specific

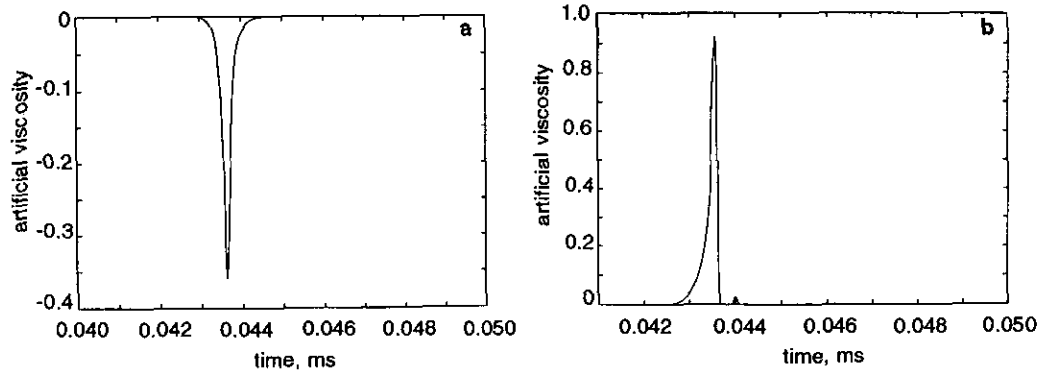

FIG. 7. Artificial viscosity for zone adjacent to wall during shock reflection: (a) amount subtracted from momentum equation to allow sharper impact by incident shock; (b) artificial viscosity entering energy equation.

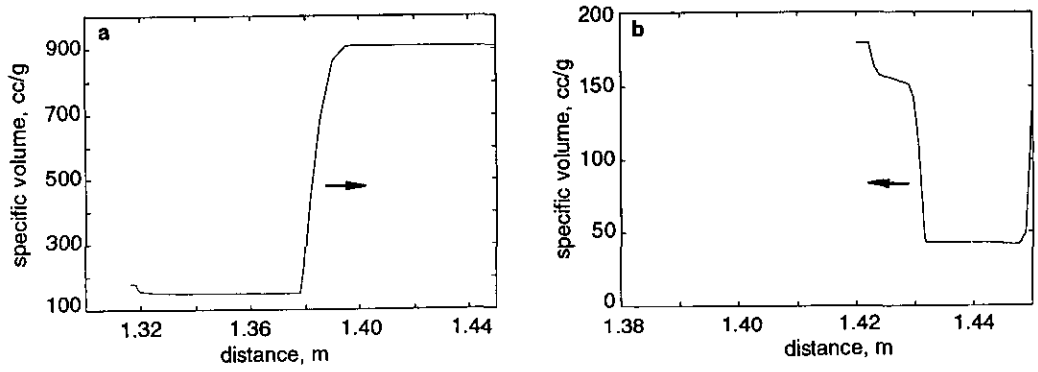

FIG. 8. Specific volumes for corresponding pressures in Fig. 5. Note error at left boundary for incident shock (a), and error at both boundaries for reflected shock (b).

volumes for the left and right boundaries are incorrect, but the solution converges to the theoretical value within about two nodes from the boundary. (We note that a characteristic treatment at these boundaries would improve this, but this is not an option in HAROLD.) This is the same for the internal energy. The calculated velocities are very smooth, although there are some long wavelength, low amplitude oscillations around zero for the reflected shock. As already noted, it is not possible for the filter to remove these. Finally, in Fig. 10 we present plots for computations involving a 100-GPa pressure jump to demonstrate the robustness of our approach. As can be seen, both incident and reflected shocks are sharp with very little oscillation, even in this extreme case.

5. SUMMARY AND CONCLUSIONS

In this paper we have discussed the implementation of the nonlinear filter, first introduced by Engquist *et al.* [6], in the context of a one-dimensional Lagrangian formulation embodied in an existing (and very old) code, and we have reported results of successful computations of very high pressure, reflected shocks. In summarizing this work, we wish to point out that there are several new and significant aspects in this research. To the authors' knowledge this is the first implementation of this nonlinear filter in conjunction with a Lagrangian formulation, and although this was not a particularly difficult part of the overall problem, it did highlight the fact that usual Roe-averaging [10] requires some modification for Lagrangian formulations. Of more importance is the treatment of reflected shocks. This has not previously been reported, at least not for the extremely high pressure shocks treated here, and it required that details of the behavior of the filter be taken into account. Namely, as noted by Shyy *et al.* [11], the filter is only able to remove short wavelength oscillations, so it was necessary to employ a boundary treatment such that high-frequency, short-wavelength oscillations are created at the boundary during the reflection and then subsequently filtered. In addition, our implementation of the Engquist filter for systems includes portions of the scalar filters described in [6] that remove plateau and zigzag effects, and it also provides a partial implementation of the requirements needed to guarantee the TVD property. To our knowledge, this is the first such implementation.

The results of our computations show that with these modifications we are able to capture very high-pressure shocks, including those that have undergone reflection from a solid boundary, and do so accurately and efficiently. In particular, even in the

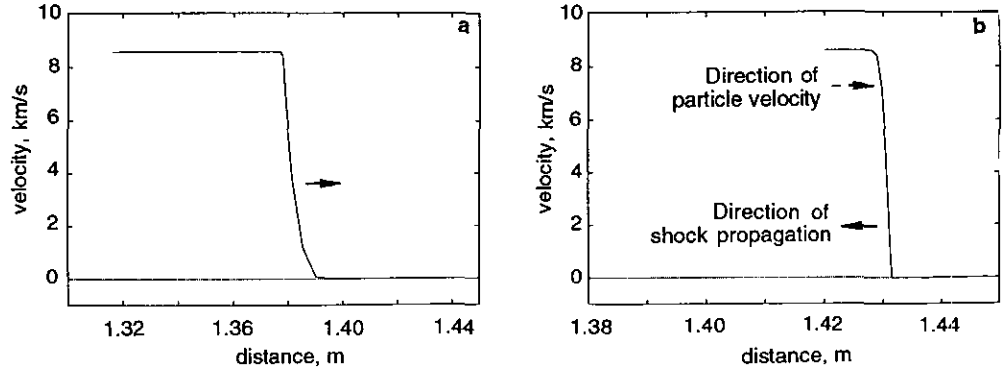

FIG. 9. Velocities for corresponding pressures of Fig. 5: (a) incident shock; (b) reflected shock.

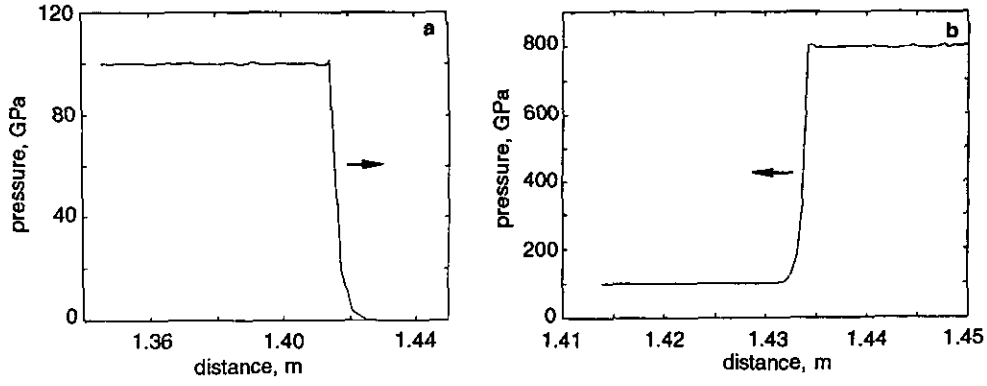

FIG. 10. One megabar pressure case: (a) incident; (b) reflected shock.

case of reflected shocks, the shock wave is captured in five to seven grid points, independent of grid spacing, and the computational expense of doing this is at most only 50% greater than that of running the basic finite difference code itself. This is approximately a factor of 2 faster than flux modification versions of TVD (cf. [3]), in agreement with timing results published in [6] and consistent with what one would expect from straightforward accounting of floating-point arithmetic. In terms of computations, this nonlinear filter in effect replaces arithmetic operations (required in other shock capturing schemes) with logic; and our experience has shown that for this problem a small amount of logic can eliminate a significant amount of arithmetic and still achieve the desired numerical accuracy.

We must emphasize, however, that these results are for one-dimensional model problems. Certainly, the ultimate test for any numerical method is application to three-dimensional problems. While specific results along these lines will be the subject of future reports, we feel it is worthwhile to comment at this time that, as discussed by Engquist *et al.* [6], the multidimensional implementations of the nonlinear filter are typically analogous to time-splitting schemes. In this regard, we expect that there may be accuracy problems to be overcome; but if this can be accomplished, the multidimensional nonlinear filter will be a highly efficient shock-capturing tool because it is applied line-by-line in each spatial direction and can thus be implemented in an "embarrassingly" parallel fashion (i.e., with a number of processors greater than or equal to the number of grid lines running in a given direction, the total time to complete filtering in that direction is the same as that needed to filter along the grid line having the most points requiring filtering). This is particularly appropriate in the context of MIMD machines having fairly significant processing power in each CPU. Moreover, because it is a postprocessor it should be relatively easy to implement, even for quite complicated three-dimensional, time-dependent codes.

ACKNOWLEDGMENT

This study is performed under the auspices of the Defense Nuclear Agency. The first author is indebted to Dr. P. Randy Rohr of the Defense Nuclear Agency for the support and several in-depth discussions.

REFERENCES

1. J. Von Neumann and R. D. Richtmyer, *J. Comput. Phys.* **21,** 232 (1950).
2. S. T. Zalesak, *J. Comput. Phys.* **31,** 335 (1979).
3. A. Harten, *J. Comput. Phys.* **49,** 357 (1983).
4. P. Colella and P. R. Woodward, *J. Comput. Phys.* **54,** 174 (1984).
5. A. Harten and S. Osher, *SIAM J. Numer. Anal.* **24,** No. 2, 279 (1987).
6. B. Engquist, P. Lotstedt, and B. Sjogreen, *Math. Comput.* **52,** No. 186, 509 (1989).
7. F. Lafon and S. Osher, *J. Comput. Phys.* **96,** 110 (1991).
8. H. L. Brode, W. Asano, M. Plemmons, L. Scantlin, and A. Stevenson, Rand Corporation Memorandum RM-5187-PR, Santa Monica, CA, 1967 (unpublished).
9. R. Courant and K. O. Friedrichs, *Vol. I, Supersonic Flow and Shock Waves* (Interscience, New York, 1948).
10. P. L. Roe, *J. Comput. Phys.* **43,** 357 (1981).
11. W. Shyy, M.-H. Chen, R. Mittal, and H. S. Udaykumar, *J. Comput. Phys.* **102,** 49 (1992).